Detiding Shipboard ADCP Data in Eastern Boundary Current

HERIBERTO JESUS VAZQUEZ, JOSE GOMEZ-VALDES, AND MODESTO ORTIZ

Physical Oceanography Department, CICESE, Ensenada, Baja California, Mexico

JUAN ADOLFO DWORAK

Instituto Tecnologico de Guaymas, Guaymas, Sonora, Mexico

(Manuscript received 10 March 2009, in final form 23 June 2010)

ABSTRACT

Spatiotemporal fitting by the least squares method is commonly applied to distinguish the mean flow from the tidal current from shipboard ADCP data in coastal ocean. To analyze this technique in a pelagic region of an eastern boundary current system, a 6-yr period of shipboard ADCP data off Baja California is examined. A diverse set of basis functions is studied and a global tidal model is used for comparison purposes. The Gaussian function together with a nodal configuration of one node in the middle and close to the coast of the region is the best option. However, to obtain the optimal solution, the geostrophic flow, which is stronger than the tidal flow and highly variable off Baja California, might be removed prior to fitting the data. In general, the semimajor axis of the tidal ellipse (M_2) is parallel to the coast and the phase speed is poleward and parallel to the coast, in agreement with Kelvin wave dynamics. Because the tides in eastern boundary currents are explained by Kelvin wave dynamics, the use of both the velocity field without geostrophic variability and the Gaussian function in the spatiotemporal fitting by least squares technique is a promising tool for detiding shipboard ADCP data from these systems.

1. Introduction

The velocity field in eastern boundary currents is regularly inferred from hydrographic and altimetry data (see, e.g., Lynn and Simpson 1987; Strub and James 1995). However, the velocity field obtained from these tools includes only the geostrophic component. Nevertheless, shipboard acoustic Doppler current profiler (ADCP) observations are becoming quite common in these systems (see, e.g., Pierce et al. 2000; Gay and Chereskin 2009); its associated velocity field includes not only the geostrophic current but also other currents, for example, wind-driven flows. Shipboard ADCP measurements contain tidal currents as well, although they are of small amplitude in eastern boundary currents (see, e.g., Munk et al. 1970), and it is necessary to detide the data in order to bring out residual flows from the undesirable signal. More importantly, because in coastal upwelling–dominated systems the seasonal variability of the geostrophic flow is regularly high (see, e.g., Lynn and Simpson 1987), this variability is contained in the ADCP data. Therefore, detiding shipboard ADCP data from observational studies in eastern boundary systems is still a challenging task.

Three methods to remove tidal currents from shipboard ADCP measurements in the coastal ocean are regularly used. One method is based on repeated passes along a given line to create a time series at selected sites (see, e.g., Simpson et al. 1990; Lwiza et al. 1991). Another method is based on predictions of tidal currents from a numerical tidal model (see, e.g., Foreman and Freeland 1991). Candela et al. (1992) introduced a two-dimensional method based on spatiotemporal fitting by a least squares method using arbitrary basis functions for extracting the spatial variations of the tidal signal. Münchow (2000) extended this method to three-dimensional fields. The spatiotemporal fitting is the most widely used (see, e.g., Steger et al. 1998; Wang et al. 2003; Carrillo et al. 2005); however, it has not been tested for systems with weak tidal current and highly variable geostrophic flow.

In the pelagic region of the California Current waters, tidal currents are about 5 cm s^{-1} (Munk et al. 1970), and the seasonal variability of the equatorward flow is high (Lynn and Simpson 1987; Strub and James 2000). For

Corresponding author address: Jose Gomez-Valdes, CICESE, Carretera Ensenada-Tijuana No. 3918, Zona Playitas, Ensenada, Baja California 22860, Mexico.
E-mail: jgomez@cicese.mx

DOI: 10.1175/2010JTECHO697.1

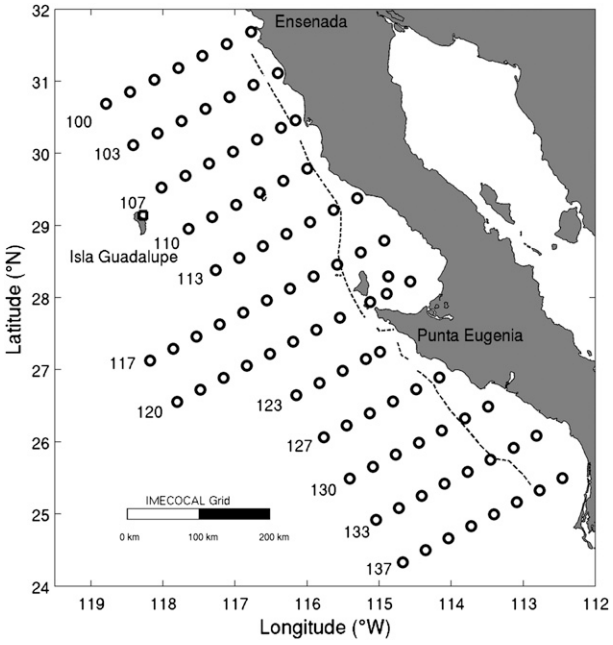

FIG. 1. The IMECOCAL sampling grid. The 1000-m isobath (dashed line) and the CTD stations (circles) are indicated. The numbers are the names of each hydrographic line. A pressure sensor was deployed in Isla Guadalupe.

example, in April the equatorward current is identified off Baja California and it is disorganized in January. Eddies and meanders are usual in summer. In this report, we examine the spatiotemporal fitting for detiding shipboard ADCP data taken off the Baja California Peninsula for the Investigaciones Mexicanas de la Corriente de California (IMECOCAL) program. Several basis functions are explored. We use a global tidal model as a tool to search for the optimal solution. In particular, the problem of the variability of the geostrophic field on the spatiotemporal fitting is addressed.

2. Data

IMECOCAL is an ongoing observational program that started during autumn of 1997, and since then it has carried out continuous quarterly surveys in the southern portion of the California Current (off Baja California) using the Centro de Investigación Científica y de Educación Superior de Ensenada, Baja California's (CICESE's) oceanographic ship, the Research Vessel (R/V) *Francisco de Ulloa*, a 28-m-long and 3-m-wide craft. We included 19 surveys in the analysis, which were carried out during the period of 2000–05. Each cruise lasted approximately 21 days. The R/V *Francisco de Ulloa* regularly departed from Ensenada (31°51′N, 116°37.5′W), Baja California, and navigated the set of 12 hydrographic lines shown in Fig. 1. Spacing between stations is ~37 km and spacing between hydrographic lines is ~74 km. At each station, conductivity–temperature–depth (CTD)/rosette casts were taken from the surface to a minimum depth of 1000 m. Temperature and conductivity sensors were factory calibrated prior to each survey. Gomez-Valdes and Jeronimo (2009) analyzed the CTD data taken from 1997 to 2007.

TABLE 1. Names and dates of cruises managed for the IMECOCAL program that were used in this study.

Cruise name	Year	Dates	No. of CTD stations	Distance traveled with ADCP (km)
0010	2000	18–31 October	86	2972
0106	2001	26 June–16 July	83	4579
0110	2001	4–23 October	88	4498
0201	2002	19 January–7 February	72	4070
0204	2002	21 April– 9 May	72	4363
0207	2002	12 July–1 August	90	4375
0304	2003	6–23 April	77	4006
0307	2003	7–28 July	77	4616
0310	2003	10–30 October	89	4388
0402	2004	31 January–19 February	68	4251
0407	2004	13–29 July	93	3858
0410	2004	10–28 October	76	3929
0504	2005	15 April–6 May	85	4326

The R/V *Francisco de Ulloa* carried a hull-mounted RD Instruments broadband 153.6-kHz ADCP at approximately 2.8 m below sea surface. The bin depth was 8 m, and the average time interval is 5–8 min. Because the sampling strategy considered a 12–24-h rest in Isla Cedros (28°10′21.49″N, 115°14′36.67″W), Mexico, the resulting analysis period was 10 days for ADCP data. The ship's underway velocity was typically 4 m s^{-1}. The first valid data bin in the profile was selected at 12-m depth. ADCP observations were screened to exclude erroneous data and then were calibrated using the method described by Joyce (1989). According to these criteria, six surveys were excluded from the analysis. The random noise was reduced by a 60-min average of the profiles. Using this procedure, we reduced the expected error from 2.5 to 0.5 cm s^{-1}. Table 1 shows names and dates of the 13 surveys in which ADCP and CTD data were collected.

3. Geostrophic current from ADCP data

Because the seasonal variability of the geostrophic flow is high off Baja California (Lynn and Simpson 1987; Strub and James 2000), it is anticipated that the geostrophic velocity field shows a unique pattern in each one of the cruises. Following Wei et al. (2008), a streamfunction was fitted to our ADCP dataset to merge out the geostrophic flow. We used a coherence scale of 220 km. Our results

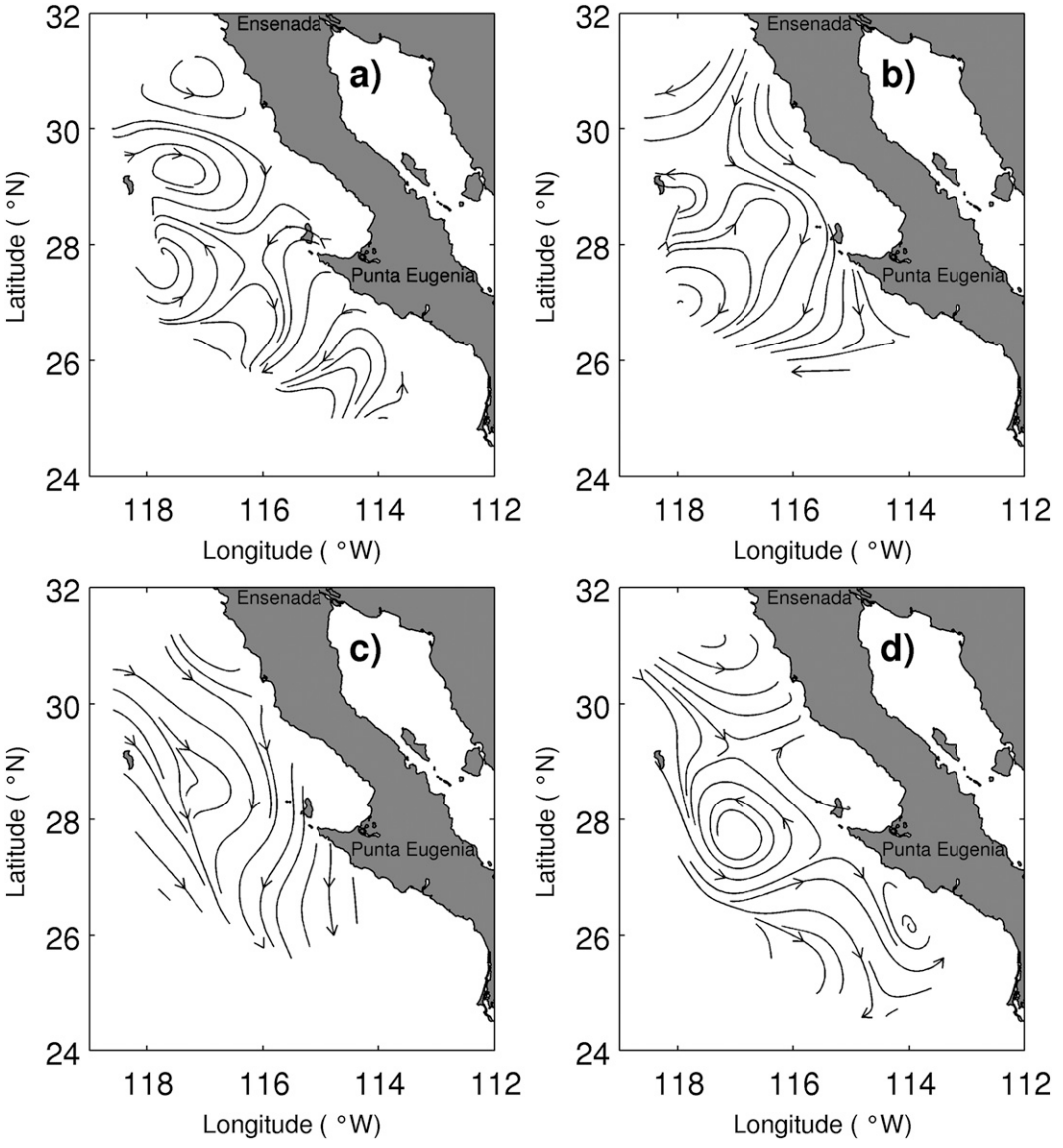

FIG. 2. Geostrophic components obtained from ADCP data (a) October 2001, (b) January 2002, (c) April 2002, and (d) July 2002.

corroborated the high variability of the geostrophic flow. Figure 2 shows geostrophic flow along 1 yr at 20-m depth. The presence of a southward flow and the dominance of mesoscale eddies are conspicuous features. In particular, the summer pattern is consistent with those reported by Strub and James (2000) and Soto-Mardones et al. (2004). There is a highlighted feature in July 2002, a cyclonic mesoscale eddy off Punta Eugenia, Baja California, which shows a ~200-km diameter. The eddy was present too in July 2004 (not shown).

To validate the geostrophic field obtained from ADCP, we used different approaches to estimate it. First, we used the common geostrophic method for CTD casts, and second we used dynamic topography from satellite altimetry [Archiving, Validation, and Interpretation of Satellite Oceanographic data (AVISO)]. We calculated the geostrophic currents from CTD data following the standard procedure. First, ΔD, where D is the dynamic height, was calculated from

$$\Delta D = -\frac{1}{10}\int_{p_1}^{p_2} \delta \, dp, \tag{1}$$

where δ is the specific volume anomaly and p is pressure. The geostrophic velocity (u, v) was obtained in

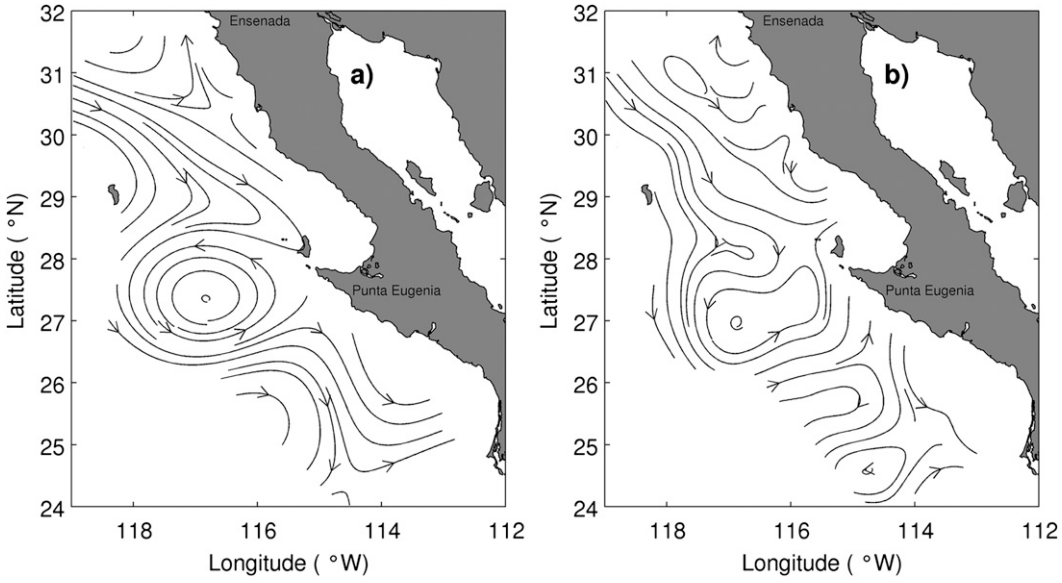

FIG. 3. Comparison between geostrophic components obtained from (a) CTD data and (b) altimetry (AVISO) for the July 2002 cruise survey.

terms of dynamic height as $fv = 10\Delta D(\Delta x)^{-1}$ and $fu = -10\Delta D(\Delta y)^{-1}$, where f is the Coriolis parameter and Δx and Δy are the horizontal distance. The regular hydrographic functions from United Nations Educational, Scientific and Cultural Organization (UNESCO) were employed. Here, 1000 dbar was chosen as the reference depth, which, although arbitrary, had been shown to be a good reference level of no motion for the California Current waters off Baja California (Jeronimo and Gomez-Valdes 2007). Following Jeronimo and Gomez-Valdes (2006), the geostrophic velocity was calculated from the optimum interpolation of the dynamic height (20/1000 dbar) field. On the other hand, we computed the geostrophic field directly from the dynamic topography obtained from AVISO. The geostrophic component from the ADCP observations compares well with the geostrophic flow obtained from CTD data. The correlation coefficient between them was 0.87. The correlation coefficient between the geostrophic flow derived from ADCP data and that derived from AVISO was 0.7. Figure 3 shows the fields from CTD at 20-m depth and from AVISO at the surface for July 2002. The two fields capture correctly the cyclonic eddy off Punta Eugenia.

4. Detiding ADCP data

Because there are no applications of the fitting method proposed by Candela et al. (1992) in eastern boundary currents, where the tidal currents are weak and the geostrophic flow shows high seasonal variability, we decided to address this problem. Our methodology is presented as follows: First, the spatial least squares technique is described. Second, the global tidal model that is used for comparison purposes is introduced. Third, the skill score to search for the best basis functions is mentioned. Finally, the problem of the high variability of the geostrophic field is discussed.

a. The fitting method

Our fitting scheme is based on the work of Candela et al. (1992) and Wang et al. (2004). The fitting scheme was implemented to the vertically integrated velocity estimated from the shipboard ADCP data. According to Candela et al. (1992), the northward velocity component (v_{ADCP}) is

$$v_{\mathrm{ADCP}}(x, y, t) = v_{\mathrm{tide}}(x, y, t) + v_{\mathrm{residual}}(x, y, t), \quad (2)$$

where v_{ADCP} is the velocity field from ADCP data, v_{tide} is the tidal velocity field, and v_{residual} is the residual velocity field. Here, v_{tide} can be expanded as a combination of trigonometric and spatially variant functions as

$$v_{\mathrm{tide}} = \sum_{i=1}^{N}[b_i(x, y)\cos(\omega_i t) + c_i(x, y)\sin(\omega_i t)], \quad (3)$$

where b_i and c_i are functions that depend on the horizontal coordinates, N is the number of resolvable tidal constituents, ω_i is the ith tidal frequency, and t is time. Both b_i and c_i are expanded in terms of a set of basis functions. A similar representation is used for the eastward velocity component.

To analyze the tidal constituents in the study area, we examined a set of sea level data from Isla Guadalupe (29°8′N, 118°16.5′W). Table 2 shows the amplitude and

TABLE 2. Amplitude (cm) and phase (°) with its respective errors and signal-to-noise ratio (SNR) for the principal tidal constituents from a pressure sensor at Isla Guadalupe. Phase referred to Greenwich time.

Tidal constituent	Amplitude (cm)	Phase (°)	Amplitude error	Phase error	SNR
O_1	17.98	191	0.36	1	2400
K_1	29.27	207	0.40	1	5500
M_2	39.53	130	0.87	1	2100
S_2	19.03	131	0.90	3	450

phase of the main tidal components, which were obtained from 1-yr observation interval using harmonic analysis following Pawlowicz et al. (2002). Calculating the form number, it was found that the tide in the zone is mixed with semidiurnal dominance. From these results, and according to Kelvin wave dynamics, the semidiurnal velocities are ~3 and ~1 cm s^{-1} for M_2 and S_2, respectively, while the diurnal velocities are ~2 and ~1 cm s^{-1} for K_1 and O_1, respectively. These results are in agreement with observed values by Munk et al. (1970), who used currents measurements in the pelagic region off California. They demonstrated that the main tidal constituents are mainly barotropic Kelvin waves and that the M_2 current is the component of the foremost importance, and the only one above the ambient noise.

Steger et al. (1998) defined a Rayleigh criterion for spatiotemporal analysis of tides

$$n\Delta t d^{-1} \geq \left|\omega_1 - \omega_2\right|^{-1}, \tag{4}$$

where n is the number of data, Δt is the interval sampling, ω_1 and ω_2 are the frequencies to be separated, and d is the dimension number. Because in our case $d = 3$, it is required to have ~77 h of continuous measurements to distinguish the diurnal band from the semidiurnal band, and ~1000 h to separate the most important semidiurnal (M_2 and S_2) and diurnal (K_1 and O_1) constituents. Because our period of analysis is ~240 h, we can only differentiate the semidiurnal band from the diurnal one. On the other hand, inertial oscillations are also captured for ADCP measurements (Garcia-Gorriz et al. 2003). These oscillations off of Baja California reach periods between 23 and 25 h, which are close to the main diurnal constituent. By applying Eq. (4), it is easy to see that we are not able to distinguish the diurnal tidal signal from the inertial oscillations. Therefore, it is most convenient to choose the M_2 for the analysis; however, the fitting is valid for the entire semidiurnal band.

Nominating functions that depend on spatial coordinates is needed in our analysis. The choice of the spatial basis function is, to some degree, arbitrary (Candela et al. 1992); there is not a method to select the best basis function.

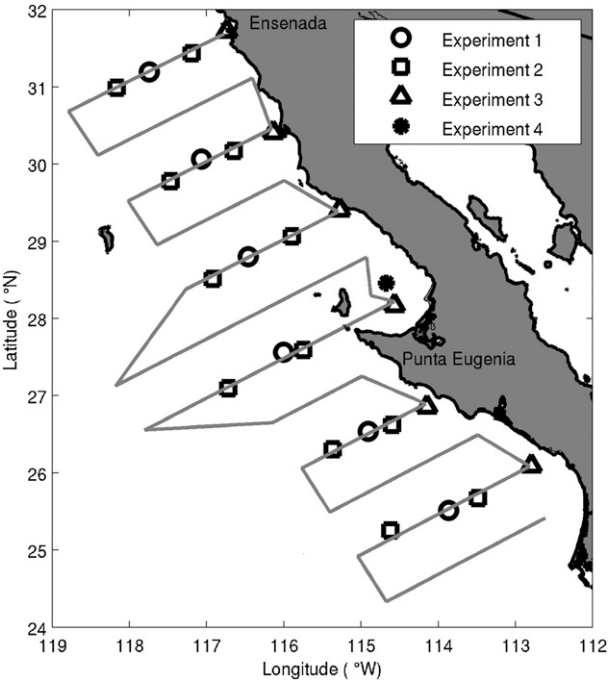

FIG. 4. The configuration of nodes for each experiment. Dotted lines indicate the R/V *Francisco de Ulloa* cruise tracks with a hull-mounted ADCP.

The knowledge of the dynamic of the tides in the study area is the best indicator of the form of the basis function (Candela et al. 1992). In this study, the following basis functions were implemented:

$$\{b_i(x, y), c_i(x, y)\} = \left\{ \begin{array}{l} \displaystyle\sum_{j=0}^{M}\sum_{m=0}^{j}(\alpha_l, \beta_l)x^{j-m}y^m \\ \displaystyle\sum_{j=1}^{k}(\alpha_j, \beta_j)|\overline{\mathbf{x}}|^2(\ln|\overline{\mathbf{x}}| - 1) \\ \displaystyle\sum_{j=1}^{k}(\alpha_j, \beta_j)e^{-(|\overline{\mathbf{x}}|^2/2L^2)} \end{array} \right\}, \tag{5}$$

where M stands for degree of the polynomial; m, j, and l are integers, where $l = (j - m, m)$; the coefficients α and β are parameters to fit by the least squares technique; k is node number; $\overline{\mathbf{x}}$ is the position vector of each observation referred to each node; and L stands for the decorrelation length scale.

Lower-order polynomial and biharmonic Green functions were employed by Candela et al. (1992), while Wang et al. (2003) used Gaussian functions. In our study, three experiments were conducted for polynomial functions by varying the degree of the polynomial in each one of the experiments, whereas four different nodal configurations (Fig. 4) were explored for biharmonic Green and

Gaussian functions. For the last two basis functions, the number and the spatial distribution of the nodes, though arbitrary, are crucial for this method (Candela et al. 1992; Münchow 2000; Wang et al. 2004). Candela et al. (1992) suggested that for the location of the nodes in biharmonic Green function it is necessary to carry out tests with different nodal configurations to find the optimal solution. Münchow (2000) found that the biharmonic Green functions are sensitive to the nodal locations. For the case of the Gaussian functions, if the nodal number increases, then the spatial resolution increases too, but at the expense of having too-few data in each estimate (Wang et al. 2003). Hence, the nodal configuration is a compromise between spatial resolution and data points in each estimate to increase robustness (Wang et al. 2003). We tested several configurations, taking in account the sampling grid.

The technique solves a system of equations of the form $\mathbf{Ac} = \mathbf{b}$, where $\mathbf{A}$ is a matrix that depends on the basis function chosen, $\mathbf{c}$ is a vector of the expansion coefficients, and $\mathbf{b}$ is a vector containing the measurements. To solve this problem, the matrix was inverted via the singular value decomposition (SVD). The singular value spectrum allows a trade-off analysis of the least squares method (Wang et al. 2004).

b. Global tidal model

For comparison purposes, we used the global numerical model of Goto et al. (1997). This model solves the Laplace tidal equations in a spherical polar system of coordinates by the finite difference method with a staggered leapfrog scheme, and it has been used widely for global tsunami propagation (see, e.g., Ortiz and Bilham 2003). The model forcing term was obtained from the tidal potential that was set for an artificial satellite revolving around the terrestrial equator for the frequency of the M_2 tidal constituent. In the computation the time step was set to 10 s, and the grid spacing to 30 min. The global bathymetry was subsampled from 2′ Gridded Earth Topography (ETOPO2) data (Smith and Sandwell 1997). The amplitude and phase of the tidal constituent resulting from the tidal model adequately reproduced the global cotidal charts as obtained from Ocean Topography Experiment (TOPEX) data (Le Provost et al. 1995). Figure 5 illustrates the resulting global M_2 cotidal chart for the northeast Pacific Ocean. In particular, the model output compared well with the amplitude and phase computed from the regional tide gauge network in Baja California.

Furthermore, this model reproduces the M_2 tidal ellipse parameters resulting from the Oregon State University (OSU) TOPEX/Poseidon global tidal model (TPXO 6.2) very well (Egbert et al. 1994; Egbert and Erofeeva 2002). Following Kundu (1976), we computed the complex correlation between the Goto et al. (1997) model and OSU TPXO output. First, we represented the tidal ellipse parameters in a complex form as follows:

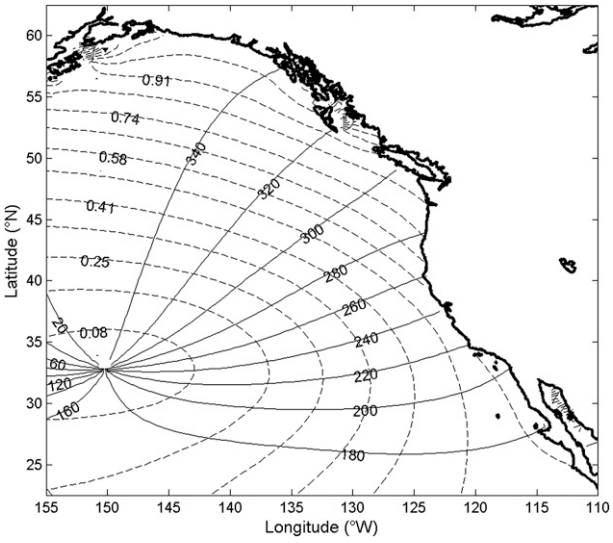

FIG. 5. Cotidal chart for the northeast Pacific Ocean obtained from the global tidal model. The phase (°, solid lines) and the amplitude (m, dotted lines) are represented.

$$w_m(x, y) = U_m(x, y)\cos[\theta_m(x, y)] + iU_m(x, y)\sin[\theta_m(x, y)], \quad (6)$$

where $w_m(x, y)$ is the complex representation for the tidal ellipse parameter for the Goto et al. (1997) model, $U_m(x, y)$ and $\theta_m(x, y)$ are the semimajor axis and the inclination of each ellipse, and $i = (-1)^{1/2}$. A similar representation was made for the OSU TPXO. Then, the correlation was obtained from

$$\rho = \frac{\langle w_m^*(x, y)w_t(x, y)\rangle}{\langle w_m^*(x, y)w_m(x, y)\rangle^{1/2}\langle w_t^*(x, y)w_t(x, y)\rangle^{1/2}}, \quad (7)$$

where the asterisk indicates the complex conjugate; m and t stands for Goto et al. (1997) model and OSU TPXO, respectively. The angle bracket denotes spatial average. We found a 0.98 correlation and a $-1°$ average inclination between the two tidal models where the sign indicates that the angle rotates anticlockwise from the second to the first vector.

c. Error skill score

As a quantitative measure of the success of the tidal currents computation by the least squares technique using several basis functions, we compared the fitting

results with the model-predicted values. The comparison was made between tidal ellipses resulting from each tool. Following Foreman and Thomson (1997), we defined the optimal solution as the minimum mean distance in the complex plane between the two sets of ellipse parameters in the form

$$E = \frac{1}{S}\sum_{i=1}^{S}\left(\left\{[U_f^i\cos(\theta_f^i) - U_m^i\cos(\theta_m^i)]^2 + [U_f^i\sin(\theta_f^i) - U_m^i\sin(\theta_m^i)]^2\right\}\right)^{1/2}, \quad (8)$$

where E is the mean distance; S is the number of tidal ellipses; U_f and U_m are the semimajor axes from the fitting and from the model, respectively; and θ_f and θ_m are the inclination of semimajor axes from the fitting and the model, respectively.

d. Removing the geostrophic flow

We have demonstrated that the variability of the geostrophic flow is high, so it might influence the spatiotemporal fitting. As a manner of "detrending" the ADCP data from that determining factor, we first removed the geostrophic flow calculated from the ADCP data for each cruise

$$v_a = v_{\mathrm{ADCP}} - v_g, \quad (9)$$

where v_a and v_g are the "detrended" (nongeostrophic) and geostrophic velocity, respectively. To separate the tidal and residual currents, spatiotemporal fitting using the least squares method was applied to the v_a field (i.e., $v_a = v_{\mathrm{tide}} + v_{\mathrm{residual}}$), such that the northward velocity component after the detiding procedure was calculated from

$$v_{\mathrm{Detide}} = v_{\mathrm{ADCP}} - v_{\mathrm{tide}}. \quad (10)$$

Figure 4 shows the nodal configuration for each experiment. We tested three polynomials—P1, P2, and P3—where P1 is a first-degree polynomial, and so on. Furthermore, G1 is a Gaussian function with nodal configuration denominated experiment 1, and B2 is a biharmonic function with nodal configuration denominated experiment 2, and so on. Table 3 shows the comparison between the fitting (observed) and model results (predicted) using E as error skill score. The best results are obtained by using experiment G4. Once we reached the best nodal configuration, we repeated the same procedure for the nongeostrophic field (v_a). We found that there is a more suitable agreement between observations and predictions using the nongeostrophic field than using the original ADCP data. In this case, E was 0.51 cm s^{-1}, which indicates an enhancement of 40%.

Figure 6 illustrates the good agreement between the resulting tidal ellipse parameters from experiment G4 using the nongeostrophic field and those predicted by the tidal model. Furthermore, the mean distance for this case is the lowest. Therefore, experiment G4, using the nongeostrophic field in the spatiotemporal fitting, resulted in the optimal solution. On the other hand, the resulting pattern and the magnitude of the M_2 tidal constituent is in agreement with the Kelvin wave dynamics reported by Munk et al. (1970). The phase for the y and x components of the tidal current is also shown in Fig. 6. It is found that the maximum velocities of the y component were reaching first in the south part and then propagated to the north. These results, together with the information provided by Fig. 5, are in agreement with the pattern of mode 25, the Pacific–North America Kelvin wave, reported by Platzman (1979).

5. Residual current

The residual (detided) flow can be divided into geostrophic and nongeostrophic components. We found that geostrophic flow is highly variable, but this explains only 25% of the total variance. The rest of the variance is explained by the nongeostrophic component. We calculated the mean perpendicular transport to each hydrographic line for the four cruises for the geostrophic and nongeostrophic components. The transport was calculated from the surface to the limit of the ADCP's resolution (124 m). Table 4 shows mean transports for the 12 hydrographic lines, where positive values indicate a poleward transport. It is noteworthy that there are not spatially coherent patterns; we suggest that this is due to

TABLE 3. Mean distance (E) between observed and predicted tidal characteristics for each experiment.

Basis functions	Mean distance (cm s^{-1})
P1	1.82
P2	1.64
P3	1.61
G1	1.22
G2	2.47
G3	1.05
G4	0.87
B1	1.21
B2	2.38
B3	1.28
B4	1.85

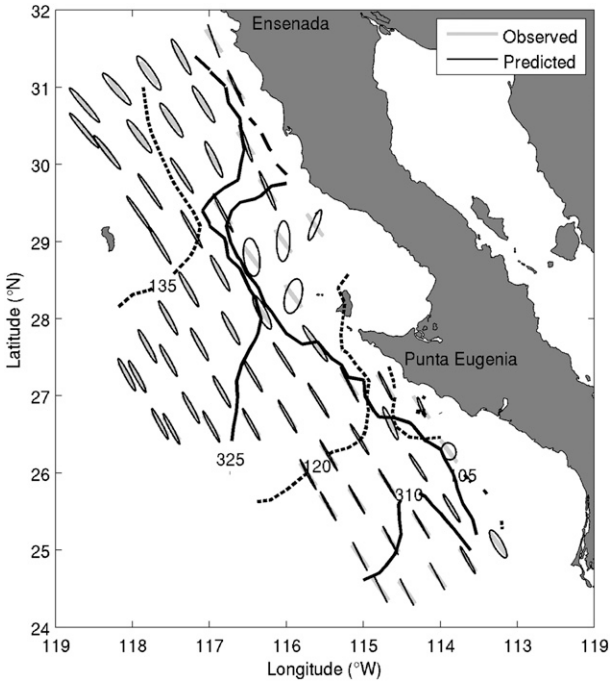

FIG. 6. Semidiurnal tidal ellipses derived from shipboard ADCP data (gray) and derived from global tidal model (black). The phase of the x (solid lines) and y (dashed lines) velocity component are indicated.

eddies and meanders, which generate complex fields. For example, we found that off northern Baja California a nongeostrophic eddy was conspicuous in the cruise of October 2001 (not shown); the same pattern was present in the geostrophic field.

It appears that the mean parallel to the coast nongeostrophic flow is related to the wind component that is parallel to the coast. By doing linear regression analysis between the mean nongeostrophic transport and the mean wind obtained from QuikSCAT, we found two features: 1) when the wind is weak, the transport is also weak, and 2) there is a change in flow direction when the wind is around 4 m s^{-1} (Fig. 7). However, the fitting only explains the 45% of the total variance. Hence, a feasibility study is needed to elucidate the main forcing mechanisms of the nongeostrophic component.

6. Discussion

The spatiotemporal fitting by least squares for detiding shipboard ADCP observations introduced by Candela et al. (1992) is mainly used in coastal ocean, where tidal currents are the most energetic motion. In this study, its implementation for the IMECOCAL dataset, which includes the southern part of the California Current, is considered. Several basis functions were examined. The optimal solution was found by comparing the least squares solutions with the predictions of a global tidal model. We found that the Gaussian was the best basis function in agreement with the findings of Wang et al. (2003), but with a different nodal configuration. They used a large number of nodes to get the best fitting and to bring out the tidal currents structure. We used a nodal configuration with only one node, which was collocated close to the coast. On the other hand, we also found that geostrophic flow variability affects the spatiotemporal fitting. We improved the performance of the fitting by subtracting the geostrophic flow from the ADCP data prior to fit the tidal current by least squares.

The Gaussian function with one node close to the coast was the best basis function because of its structure. Along

TABLE 4. Mean geostrophic and nongeostrophic (G and A, respectively) transports [1 Sv $\equiv 10^6$ m^3 s^{-1} (Sv)] perpendicular to each hydrographic line.

	October 2001		January 2002		April 2002		July 2002	
Lines	G	A	G	A	G	A	G	A
100	−0.15	0.05	−0.02	0.06	−0.01	0.10	−0.01	0.05
103	0.05	−0.01	−0.03	−0.02	0.00	0.05	0.02	0.01
107	0.08	−0.07	0.03	0.09	−0.02	0.06	0.04	0.00
110	0.01	0.02	0.06	−0.08	−0.03	0.03	0.00	0.07
113	0.00	−0.08	0.01	−0.08	−0.03	0.00	0.02	−0.16
117	0.04	−0.07	−0.03	0.09	−0.05	0.13	−0.02	0.04
120	0.07	−0.06	−0.08	0.16	−0.08	0.23	0.03	0.02
123	−0.05	0.06	−0.05	0.08	−0.13	0.33	0.06	−0.19
127	−0.05	0.10	−0.03	0.02	−0.06	0.02	−0.02	0.00
130	0.01	−0.12	−0.01	−0.04	−0.05	0.07	−0.09	0.14
133	0.06	−0.10	No data	No data	No data	No data	−0.05	0.24
137	−0.04	0.03	No data	No data	No data	No data	0.14	−0.30

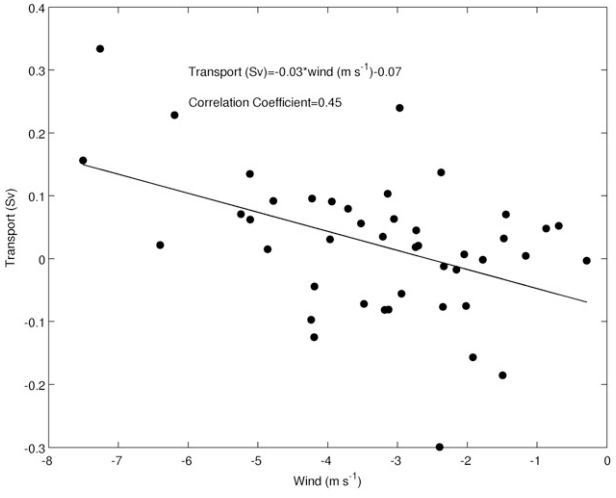

FIG. 7. Relationship between alongshore transport and alongshore wind (positive poleward).

the west coast of Baja California, the spatial structure of the principal tidal constituents is in agreement with a Kelvin wave (Munk et al. 1970). Furthermore, Platzman (1979) showed that the normal mode of a 15.5-h period is described as a Kelvin wave in the eastern Pacific Ocean. Thus, the optimal space basis function for this region is a Gaussian function. In eastern boundary currents the main tidal constituents are explained by the dynamics of these waves (Platzman et al. 1981; Le Provost et al. 1995). Thus, our methodology, which although particular for pelagic ADCP measurements off Baja California, might be applicable to any eastern boundary current.

The tidal currents in the IMECOCAL region are weak but are detected by the ADCP. With our methodology, it was possible to distinguish tidal currents from the mean flow. In general, part of the variability in the estimated velocity is random, so the error is reduced by averaging (Chereskin and Roemmich 1991). In our case, by using the Joyce (1989) calibration procedure and the 60-min average the error was reduced to $\sim$0.5 cm s^{-1}. The magnitude of the tidal current was $\sim$2 cm s^{-1} for the M_2 tidal constituent, which is above the noise level. Munk et al. (1970) reported the same value in the open ocean off southern California. They also reported that the northward tidal flow was parallel to the coast and that it was mainly barotropic. These observations are in agreement with our results.

The geostrophic part of the ADCP observations compares well with the geostrophic flow (20/1000 dbar) obtained from CTD and altimetry data from AVISO. In the seminal work of Lynn and Simpson (1987), the seasonal variation of the mean dynamic height (0/500 dbar) was established for the California Current system. They showed that in July the main core of the California Current is located offshore and the southern California eddy is formed. These features are also observed in our Fig. 2. Furthermore, the upper-ocean mesoscale cyclone eddy off Punta Eugenia reported by Strub and James (2000) from altimetry-derived data is also detected here from shipboard ADCP data.

Because there are many possible interactions (i.e., between wind-driven currents and coastal boundaries) and also submesoscale features (i.e., streamers), the resulting nongeostrophic pattern is complex. Therefore, it is necessary to examine the nature of the flow after extracting tidal and geostrophic currents with our methodology in a further study.

Acknowledgments. This work is a part of the Ph. D dissertation of HJV-P. The study was partly supported by grants from CONACyT, México: 82529, 23947, and 47044, and from SEMARNAT-CONACyT: 23804 and CICESE. HJV-P had a fellowship from CONACyT, México. We thank the captain and crew of the R/V *Francisco de Ulloa* of CICESE. We also thank Julio Candela, Gilberto Jerónimo, Joaquín García, and José María Robles for many helpful discussions of the problem. Bernardo Gómez edited the paper. We thank the anonymous reviewers for their valuable and helpful comments.

REFERENCES

Candela, J., R. C. Beardsley, and R. Limeburner, 1992: Separation of tidal and subtidal currents in ship-mounted acoustic Doppler current profiler observations. *J. Geophys. Res.,* **97,** 769–788.

Carrillo, L., A. J. Souza, A. E. Hill, J. Brown, L. Fernand, and J. Candela, 2005: Detiding ADCP data in a highly variable shelf sea: The Celtic Sea. *J. Atmos. Oceanic Technol.,* **22,** 84–97.

Chereskin, T. K., and D. Roemmich, 1991: A comparison of measured and wind-derived Ekman transport at 11°N in the Atlantic Ocean. *J. Phys. Oceanogr.,* **21,** 870–878.

Egbert, G., and S. Y. Erofeeva, 2002: Efficient inverse modeling barotropic ocean tides. *J. Atmos. Oceanic Technol.,* **19,** 183–204.

——, A. Bennett, and M. G. G. Foreman, 1994: TOPEX/Poseidon tides estimated using a global inverse model. *J. Geophys. Res.,* **99,** 24 821–24 852.

Foreman, M. G. G., and H. J. Freeland, 1991: A comparison of techniques for tide removal from ship-mounted acoustic Doppler measurements along the southwest coast of Vancouver Island. *J. Geophys. Res.,* **96,** 17 007–17 021.

——, and R. E. Thomson, 1997: Three-dimensional model simulations of tides and buoyancy currents along the West Coast of Vancouver Island. *J. Phys. Oceanogr.,* **27,** 1300–1325.

Garcia-Gorriz, E., J. Candela, and J. Font, 2003: Near-inertial and tidal currents detected with a vessel-mounted acoustic Doppler current profiler in the western Mediterranean Sea. *J. Geophys. Res.,* **108,** 3164, doi:10.1029/2001JC001239.

Gay, P. S., and T. K. Chereskin, 2009: Mean structure and seasonal variability of the poleward undercurrent off southern California. *J. Geophys. Res.,* **114,** C02007, doi:10.1029/2008JC004886.

Gomez-Valdes, J., and G. Jeronimo, 2009: Upper mixed layer temperature and salinity variability in the tropical boundary of the California current, 1997-2007. *J. Geophys. Res.,* **114,** C03012, doi:10.1029/2008JC004793.

Goto, C., Y. Ogawa, N. Shuto, and F. Imamura, 1997: IUGG/IOC TIME Project: Numerical method of tsunami simulation with the leap-frog scheme. UNESCO Intergovernmental Oceanographic Commission, Manuals and Guides No. 35, 126 pp. [Available online at http://www.jodc.go.jp/info/ioc_doc/Manual/122367eb.pdf.]

Jeronimo, G., and J. Gomez-Valdes, 2006: Mean temperature and salinity along an isopycnal surface in the upper ocean off Baja California. *Cienc. Mar.,* **32,** 663–671.

——, and ——, 2007: A subsurface warm-eddy off northern Baja California in July 2004. *Geophys. Res. Lett.,* **34,** L06610, doi:10.1029/2006GL028851.

Joyce, T. M., 1989: On in situ "calibration" of shipboard ADCPs. *J. Atmos. Oceanic Technol.,* **6,** 169–172.

Kundu, P. K., 1976: Ekman veering observed near the ocean bottom. *J. Phys. Oceanogr.,* **6,** 238–242.

Le Provost, C., A. F. Bennet, and D. E. Cartwright, 1995: Ocean tides for and from TOPEX/Poseidon. *Science,* **267,** 639–642.

Lwiza, K. M. M., D. G. Bowers, and J. H. Simpson, 1991: Residual and tidal flow at a tidal mixing front in the North Sea. *Cont. Shelf Res.,* **11,** 1379–1395.

Lynn, R. J., and J. J. Simpson, 1987: The California Current System: The seasonal variability of physical characteristics. *J. Geophys. Res.,* **92,** 12 947–12 966.

Münchow, A., 2000: Detiding three-dimensional velocity survey data in coastal waters. *J. Atmos. Oceanic Technol.,* **17,** 736–749.

Munk, W., F. Snodgrass, and M. Wimbush, 1970: Tides off-shore: Transition from California coastal to deep-sea waters. *Geophys. Fluid Dyn.,* **1,** 161–235.

Ortiz, M., and R. Bilham, 2003: Source area and rupture parameters of the 31 December 1881 M_w = 7.9 Car Nicobar earthquake estimated from tsunamis recorded in the Bay of Bengal. *J. Geophys. Res.,* **108,** 2215, doi:10.1029/2002JB001941.

Pawlowicz, R., B. Beardsley, and S. Lentz, 2002: Classical tidal harmonic analysis including error estimates in MATLAB using T_TIDE. *Comput. Geosci.,* **28,** 929–937.

Pierce, S. D., R. L. Smith, P. M. Kosro, J. A. Barth, and C. D. Wilson, 2000: Continuity of the poleward undercurrent along the eastern boundary of the mid-latitude north Pacific. *Deep-Sea Res. II,* **47,** 811–829.

Platzman, G. W., 1979: A Kelvin wave in the eastern Pacific Ocean. *J. Geophys. Res.,* **84,** 2525–2528.

——, G. A. Curtis, K. S. Hansen, and R. D. Slater, 1981: Normal modes in the world ocean. Part II: Description of modes in the period range 8 to 80 hours. *J. Phys. Oceanogr.,* **11,** 579–603.

Simpson, J. H., E. G. Mitchelson-Jacob, and A. E. Hill, 1990: Flow structure in a channel from an acoustic Doppler current profiler. *Cont. Shelf Res.,* **10,** 589–603.

Smith, W. H. F., and D. T. Sandwell, 1997: Global sea floor topography from satellite altimetry and ship depth soundings. *Science,* **227,** 1956–1962.

Soto-Mardones, L., A. Parés-Sierra, J. Garcia, R. Durazo, and S. Hormazabal, 2004: Analysis of the mesoscale structure in the IMECOCAL region (off Baja California) from hydrographic, ADCP and altimetry data. *Deep-Sea Res. II,* **51,** 785–798.

Steger, J. M., C. A. Collins, F. B. Schwing, M. Noble, N. Garfield, and M. T. Steiner, 1998: An empirical model of the tidal currents in the Gulf of Farallones. *Deep-Sea Res.,* **45B,** 1471–1505.

Strub, P. T., and C. James, 1995: The large-scale summer circulation of the California Current. *Geophys. Res. Lett.,* **22,** 207–210.

——, and ——, 2000: Altimeter-derived variability of surface velocities in the California Current System: 2. Seasonal circulation and eddy statistics. *Deep-Sea Res.,* **47,** 831–870.

Wang, Y.-H., S. Jan, and D.-P. Wang, 2003: Transports and tidal current estimates in the Taiwan Strait from shipboard ADCP observations (1999-2001). *Estuarine Coastal Shelf Sci.,* **57,** 193–199.

——, L.-Y. Chiao, K. M. M. Lwiza, and D.-P. Wang, 2004: Analysis of flow at the gate of Taiwan Strait. *J. Geophys. Res.,* **109,** C02025, doi:10.1029/2003JC001937.

Wei, J., D.-P. Wang, and C. N. Flagg, 2008: Mapping Gulf Stream warm core rings from shipboard ADCP transects of the Oleander Project. *J. Geophys. Res.,* **113,** C10021, doi:10.1029/2007JC004694.